JCTC Journal of Chemical Theory and Computation

New Algorithms for Optimizing and Linking Conical Intersection Points

Fabrizio Sicilia,[§] Lluís Blancafort,*[,†] Michael J. Bearpark,[§] and Michael A. Robb*[,§]

Department of Chemistry, Imperial College, London SW7 2AZ, United Kingdom, and Institut de Quimica, Computational and Departament de Quimica, Universitat de Girona, E-17071 Girona, Spain

Received September 21, 2007

Abstract: In this paper we present two new algorithms to study the extended nature of the crossing seam between electronic potential energy surfaces. The first algorithm is designed to optimize conical intersection geometries: both minima and saddle points. In addition, this method will optimize conical intersection geometries using arbitrary geometrical constraints. We demonstrate its potential on different crossing seams of benzene, *z*-penta-3,5-dieniminium, and 1,3-butadiene. The second algorithm is designed to explicitly compute the intersection-space minimum energy coordinate. Our computations show how an intersection seam and the energy along it can be unambiguously defined. A finite region of the S_0/S_1 1,3-butadiene crossing seam has been mapped out, and a new saddle point linked with two lower-lying geometries on the seam.

1. Introduction

In the past two decades conical intersection geometries have been shown to play a central role in our understanding of photochemical reactions (see for instance refs 1−3). Up to now, numerous conical intersection structures have been located and shown to be involved in several nonradiative processes (see for instance refs 1−4).

Conical intersections are not isolated points but rather are connected along an (*n*-2)-dimensional hyperline, where *n* is the number of internal degrees of freedom. Recent studies have shown that decay can also occur at higher energy points along the crossing hyperline (see for example refs 5 and 6) away from its minimum. Thus, an accurate investigation of the intersection space,[7] which is the space where the two electronic states are degenerate, becomes crucial.

In this spirit, we recently developed a new methodology to compute the curvature of the crossing seam energy, such that saddle points could be distinguished from minima within the intersection space.[8,9] In addition, from these frequency calculations we could compute the motions corresponding to any imaginary frequencies. These intersection-space vibrational modes[9] were then used to suggest connections among several conical intersection points belonging to the same intersection space. In this paper, we describe two complementary tools to study the intersection space. The first is a new algorithm designed to optimize conical intersection structures with improved convergence and which can make use of analytic second derivatives of the seam energy. The second method is for computing the minimum energy path connecting three conical intersection structures, e.g., two minima and a saddle point along the crossing seam. Thus, with the new algorithms described in this paper we have a complete set of tools capable of investigating the energy within the intersection space in the same way that one would study a single Born-Oppenheimer potential energy surface, i.e., using geometry optimization, frequency calculation, and reaction path computations (see for instance ref 10).

Over the years, many different approaches have been proposed to optimize structures where two electronic states become degenerate. The algorithms currently available are based upon either Lagrange-Newton methods (see for example refs 11−13) or projection methods (see for instance refs 14 and 15). The algorithms belonging to the first class

* Corresponding author e-mail: mike.robb@imperial.ac.uk (M.A.R.), lluis.blancafort@udg.edu (L.B.).

† Universitat de Girona.

§ Imperial College.

10.1021/ct7002435 CCC: $40.75
Published on Web 01/18/2008

have the common feature of using variations of the classical Lagrange multipliers method.[16−18] Recently, it has been shown[19] that this class of algorithms is generally very efficient. Together with a higher computational cost, these methods are, however, difficult to be efficiently implemented and improved.[19−21] One of the main problems is related to the Lagrange Hessian, which is not positive definite, i.e., for each constraint a negative eigenvalue arises. Therefore efficient updating methods such as the Broyden-Fletcher-Goldfarb-Shanno (BFGS) scheme cannot be employed, and the overall algorithm may be affected in terms of efficiency and convergence rate (see for instance refs 16, 17, 19, 20, 22, and 23). In contrast, the projection methods are designed to reach the energy degeneracy by means of a displacement within the branching space,[7] while optimizing simultaneously the energy of the excited state within the intersection space.[7]

A typical algorithm, based on projection matrices, uses a gradient composed of two distinct parts.[14] The first part consists of the normalized gradient difference vector, which is one of the two first-order degeneracy lifting directions,[1] weighted by twice the energy gap. This term is responsible for minimizing the energy difference between the two crossing states. The second part of the gradient optimizes the excited-state energy within the intersection space. Thus a critical point on the intersection hyperline can be located.

The use of a projection matrix ensures the orthogonality between the two parts of the composite gradient. However, such orthogonality may be lost in computing a quasi-Newton−Raphson displacement, as a consequence of an ill-conditioned approximate Hessian (see for instance ref 24). In other words, the displacement computed may have components in both branching and intersection space. This problem becomes troublesome in the region where the two electronic states become almost degenerate, where the displacement components within the branching plane will lift the degeneracy. The algorithm described in this paper therefore uses a combination of displacements taken within the two orthogonal spaces rather than two gradients. Although this idea is related to the theoretical development originally proposed by Anglada et al.[22] and recently reviewed and extended by De Vico et al.,[20] the actual implementation of the proposed algorithm is substantially different, as we will discuss in the next section.

In the present algorithm, as the energy difference drops below a set threshold, a Newton−Raphson displacement, taken within the intersection space, is combined with a step along the gradient difference vector. When the energy is above the given threshold, the standard projection method[14] is used. As we will discuss in section 4, the proposed algorithm shows a faster and smoother overall convergence to the minimum conical intersection geometry when compared with two previously reported algorithms.[14,22] In addition, our implementation enables one to optimize conical intersection geometries along a selected constrained redundant internal coordinate.[25−27] Finally, this algorithm and the possibility of computing analytically an intersection-space Hessian[9] can be combined with the transition state search algorithm (for a recent review see for instance ref 10) implemented in the Gaussian package.[28] To summarize, the algorithm proposed in this paper is capable of locating both minima and saddle points within the intersection space, as well as of optimizing conical intersection points along a given constrained geometrical variable.

Using two independent displacements, one within the intersection space and one along the gradient difference vector, we have also designed a method to compute a coordinate analogous to the intrinsic reaction coordinate[29−31] but confined to the intersection space. Although such a coordinate may be not physically meaningful (see for example ref 32 and following comments), it represents a unique way to define finite portions of the intersection space. In section 4, we will present the study carried out to link a new saddle point found on the S_0/S_1 crossing seam of 1,3-butadiene with two lower lying critical points on the conical intersection seam.

2. Theory

Optimization of Stationary Points along a Crossing Seam. At a conical intersection point, a displacement along two directions is capable of lifting the degeneracy at first order: the gradient difference [eq 1a] and the interstate coupling [eq 1b] (see for example refs 1, 3, 11, 33, and 34).

$$\mathbf{x}_1 = \frac{\partial(E_2 - E_1)}{\partial \mathbf{q}} \tag{1a}$$

$$\mathbf{x}_2 = \left\langle \mathbf{C}_1 \middle| \frac{\partial \mathbf{H}}{\partial \mathbf{q}} \middle| \mathbf{C}_2 \right\rangle \tag{1b}$$

In eq 1, $\mathbf{C_1}$ and $\mathbf{C_2}$ are the CI eigenvectors in the MC−SCF problem. The vectors $\mathbf{x_1}$ and $\mathbf{x_2}$ span the branching plane,[7] also referred to as the *g*-*h* plane.[3] In the orthogonal (*n*-2) subspace, the intersection space,[7] the degeneracy is retained at the first order.[9,33,35,36] The adiabatic energies of the two electronic states are indicated by E_1 and E_2, whereas **H** and **q** represent the electronic CI Hamiltonian matrix and the nuclear coordinates, respectively.

In the direct algorithm proposed by Bearpark et al.,[14] the gradient used in the optimization is the following

$$\mathbf{g} = \mathbf{f} + \mathbf{g}_p \tag{2a}$$

where

$$\mathbf{f} = 2(E_2 - E_1)\frac{\mathbf{x}_1}{\delta\kappa} = 2\Delta E\, \hat{\mathbf{x}}_1 \tag{2b}$$

and

$$\mathbf{g}_p = \mathbf{P}\frac{\partial E_2}{\partial \mathbf{q}} \tag{2c}$$

In eq 2, $\delta\kappa$ is the length of the gradient difference vector, i.e., $\delta\kappa = \sqrt{\mathbf{x}_1^T\mathbf{x}_1}$; and **P** represents the projector matrix which projects the gradient of the upper state ($\partial E_2/\partial \mathbf{q}$) onto the subspace perpendicular to the plane ($\hat{\mathbf{x}}_1$,$\hat{\mathbf{x}}_2$):

$$\mathbf{P} = \mathbf{1} - \hat{\mathbf{x}}_1\hat{\mathbf{x}}_1^T - \hat{\mathbf{x}}_2\hat{\mathbf{x}}_2^T \tag{2d}$$

The "hat" notation indicates a normalized vector. Here, we assume that the two potential energy surfaces cross each other along an (n-2)-dimensional intersection space, where n is the number of internal coordinates. However, this algorithm works also when the nonadiabatic interstate coupling vector [eq 1b] is zero by symmetry, e.g., the intersection space is of (n-1) dimensionality. For what follows, it is also worth noting that the projected gradient of the excited-state energy is the same vector as that obtained by projecting the average of the two state gradients (for the proof see the Appendix). This equivalence will be crucial in defining the second-derivative matrix of the seam energy.

An updated Hessian can become ill-conditioned in certain regions of the potential energy surface, if the composite gradient [eq 2] is used throughout the optimization. When the energy difference is large, for instance, the Hessian is dominated by contributions arising from the branching plane.[16,23,24] As a result, the degeneracy region is rapidly reached. However, when the seam is located, contributions from the branching plane to the approximate Hessian may not vanish and therefore the degeneracy is lifted.

To improve the convergence of this algorithm we therefore propose to project both gradient and Hessian when the seam region is approached, so that the possible branching-space contamination is avoided. When the energy difference is below a certain threshold, we will combine an intersection-space displacement with a step taken along the gradient difference.

For the combined step part, the potential energy within the intersection space can be described by a Taylor expansion truncated at the second-order:

$$E_{Seam} = E_{Seam}{}^0 + (\Delta\mathbf{q}_{IS}{}^0)^T\mathbf{g}_{IS}{}^0 + \frac{1}{2}(\Delta\mathbf{q}_{IS}{}^0)^T\mathbf{H}_{IS}{}^0\Delta\mathbf{q}_{IS}{}^0 \tag{3a}$$

Notice that $\Delta\mathbf{q}_{IS}{}^0 = \mathbf{q}_{IS} - \mathbf{q}_{IS}{}^0$ is an n-dimensional vector. The zero-order term is taken as the reference point and set to zero. The seam energy gradient within the intersection space, $\mathbf{g}_{IS}$, is computed as the projected average gradient (see the Appendix). This gradient allows us to introduce the intersection-space Hessian, recently proposed elsewhere,[8,9] as the second-derivative matrix of the seam energy. Defining the intersection-space Hessian of the seam energy as the projected "derivative" of the seam energy gradient, we obtain

$$\mathbf{W}_{IS} = \mathbf{P}\left[\frac{\partial}{\partial\mathbf{q}}\mathbf{g}_{IS}\right]\mathbf{P} = \frac{1}{2}\mathbf{P}\left[\frac{\partial}{\partial\mathbf{q}}\mathbf{P}\frac{\partial(E_2+E_1)}{\partial\mathbf{q}}\right]\mathbf{P} = \frac{1}{2}\mathbf{P}\left[\frac{\partial^2(E_2+E_1)}{\partial\mathbf{q}^2} - \frac{\lambda_{x_1}}{\delta\kappa}\frac{\partial^2\Delta E}{\partial\mathbf{q}^2} - \frac{\lambda_{x_2}}{\kappa_{12}}\frac{\partial^2 H_{12}}{\partial\mathbf{q}^2}\right]\mathbf{P} \tag{3b}$$

In the differentiation we have used the definition of projection matrix reported in eq 2d. We have also introduced $\lambda_{x_{1(2)}}$ to indicate the components of the average gradient along the unit gradient difference (nonadiabatic interstate coupling vector) and $\delta\kappa$ (κ_{12}) for the length of the gradient difference (nonadiabatic interstate coupling vector).

To compute the Newton−Raphson displacement, the inverse of this Hessian matrix is required. However due to the projection, $\mathbf{W}_{IS}$ has two zero eigenvalues corresponding to the branching plane directions and therefore its inverse is not defined. However, using the idea of Peng et al.,[37] one can use instead the following matrix

$$\mathbf{H}_{IS} = \mathbf{W}_{IS} + (\mathbf{1}-\mathbf{P})\mathbf{A}(\mathbf{1}-\mathbf{P}) \tag{3c}$$

where $\mathbf{A}$ is diagonal matrix whose elements are set to a large constant (e.g., 1000) and $\mathbf{P}$ is the usual projection matrix defined in eq 2d. Consequently, using the Newton−Raphson method, the intersection-space displacement can be computed as

$$\Delta\mathbf{q}_{IS}{}^0 = -(\mathbf{H}_{IS}{}^0)^{-1}\mathbf{g}_{IS}{}^0 \tag{4a}$$

Although the displacement is an n-dimensional vector, the possible contributions from the branching plane have been projected out.

To guarantee the degeneracy, the following step along the gradient difference

$$\Delta\mathbf{q}_{BS}{}^0 = (\Delta E_0/\delta\kappa_0)\hat{\mathbf{x}}_1{}^0 \tag{4b}$$

is added to $\Delta\mathbf{q}_{IS}{}^0$, so that the total displacement is given by

$$\Delta\mathbf{q}_0 = \Delta\mathbf{q}_{IS}{}^0 + \Delta\mathbf{q}_{BS}{}^0 \tag{4c}$$

Although in principle the Hessian matrix, $\mathbf{W}$, could be analytically computed,[8,9] an approximated Hessian ($\mathbf{F}$) is initially used in practice. Using the Broyden-Fletcher-Goldfarb-Shanno (BFGS) scheme, this matrix is calculated as

$$\mathbf{W} \approx \mathbf{F} = \mathbf{F}^0 + \frac{\Delta\mathbf{h}_0(\Delta\mathbf{h})_0^T}{\Delta\mathbf{h}_0^T\Delta\mathbf{q}_0} - \frac{\mathbf{F}^0\Delta\mathbf{q}_0\Delta\mathbf{q}_0^T\mathbf{F}^0}{\Delta\mathbf{q}_0^T\mathbf{F}^0\Delta\mathbf{q}_0} \tag{5}$$

Here $\Delta\mathbf{h}_0$ is computed as the difference between the gradients evaluated at $\mathbf{q}$ (current iteration) and at $\mathbf{q}_0$ (previous iteration). $\Delta\mathbf{q}_0$ represents instead the difference between the current and previous geometry. Depending on the energy gap, the gradient used in the update scheme varies as shown in Table 1.

Table 1. Relevant Quantities Used in the Presented Conical Intersection Optimization Algorithm

$\Delta E = E_2 - E_1$	>threshold[a]	<threshold
gradient[b]	$\mathbf{g} = \mathbf{f} + \mathbf{g}_{IS}$[c]	$\mathbf{g} = \mathbf{g}_{IS}$
total displacement	$\Delta\mathbf{q} = -(\mathbf{W})^{-1}\mathbf{g}$	$\Delta\mathbf{q} = -(\mathbf{H}_{IS})^{-1}\mathbf{g}_{IS} + (\Delta E/\delta\kappa)\hat{\mathbf{x}}_1$[d]

[a] The default cutoff has been set to 5×10^{-3} E_h. [b] This gradient is used to both update the Hessian matrix and to compute the displacement. [c] Defined in eq 2. [d] Defined in eq 4.

In Table 1, we have reported the main features of the algorithm discussed in this paper. The reader may recognize some similarities between the proposed algorithm and the one obtained by Anglada et al.,[20,22] who have suggested applying the Han-Powell method[16,17,23,38] to optimize conical intersection geometries. In proximity to the crossing seam, the two methodologies, for instance, use the same gradient (see the Appendix) to update the Hessian matrix, $\mathbf{F}$ [eq 5]. Moreover, the intersection-space Hessian $\mathbf{W}_{IS}$, used here, is similar to the reduced Hessian reported by Anglada et al.

Despite the various similarities, the proposed algorithm differs from the one reported by Anglada et al. in several crucial ways. First, their method uses the Hessian only to compute the intersection space displacement throughout the optimization. Consequently, the method is known (see for example refs 16, 20, and 23) to have a fairly slow convergence when one starts from a point too far away from the solution. In our algorithm, a composite gradient [eq 2] is used to compute both the displacement and to update the Hessian in regions far away from the degeneracy. Furthermore, in the seam region, the two proposed displacements differ in the form of the gradient used: we use the projected gradient [eq 2c], whereas Anglada et al. propose using the reduced gradient. However, as theoretically outlined by Nocedal et al.[23] and based on our own experience, the additional term present in the reduced gradient does not provide any benefit to the overall convergence, once the crossing region is reached. Finally, the intersection-space Hessian, $\mathbf{W}_{IS}$, shown in eq 3b, is a symmetric n by n matrix, whereas the reduced Hessian used by Anglada et al. has dimension (n-2) by (n-2). Nevertheless, it should be remarked that both matrices have the same (n-2) rank, i.e., both matrices have (n-2) nonzero eigenvalues.

Along with minimum energy crossing points, the proposed algorithm is also able to optimize different conical intersection structures along a constrained coordinate. We have recently proposed an implementation to carry out this type of optimization,[25] which prevents the possible occurrence of cancellation errors.[25−27] In that study, we suggested to apply first the constraints and subsequently to project out the branching space directions from the gradient. This procedure allowed us to map out successfully a region of the S_0/S_1 fulvene crossing seam. Nevertheless in that study, we explicitly applied symmetry considerations to carry out the calculations. Here, we apply the constraints to both branching plane vectors [eq 1], and then we build the projection matrix **P** [eq 2d]. Thus, the procedure has been generalized and implemented in a development version of Gaussian.[28] We recognize that other methodologies (see for example ref 18) which allow geometrical constraints in a conical intersection optimization algorithm have been previously reported. While these methods do not suffer from cancellation errors, they are computationally more demanding than the algorithm discussed in this paper.[19]

Finally, we have explored the possibility of combining this new algorithm with the methodology implemented in Gaussian to find transition state structures [see for example ref 10 and references therein]. Routinely, to compute a transition structure, one must compute the Hessian at a point located close enough to the quadratic region of the first-order saddle point. This matrix must have one negative eigenvalue, and the corresponding eigenvector should be a suitable guess for the initial optimization direction. In this work, we follow the same procedure but it has been limited to the intersection space. Consequently, we begin by analytically computing the intersection-space Hessian[8,9] at an approximately converged conical intersection geometry. During the rest of the optimization, the intersection-space Hessian, $\mathbf{W}_{IS}$, is updated using Bofill's scheme[39] implemented in Gaussian and then used as described above. This methodology has allowed us to locate a new saddle point in the intersection space of 1,3-butadiene.

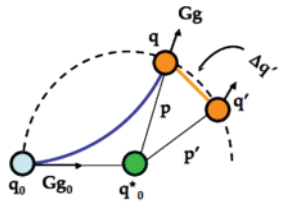

Figure 1. A graphical representation of the vectors used in the original IRC algorithm[31] is shown.

Table 2. Terms Appearing in the Single-Surface, Minimum Energy Path Algorithm of Gonzalez et al.,[31] and Their Equivalents in the Intersection-Space Version[a]

single surface[27]	intersection space
$\Delta\mathbf{q}_M = \mathbf{G}^{-1/2}\Delta\mathbf{q}$	${}^{IS}\Delta\mathbf{q}_M = \mathbf{G}^{-1/2}\Delta\mathbf{q}_{IS}$
$\mathbf{g}'_M = \mathbf{G}^{1/2}\mathbf{g}'$	${}^{IS}\mathbf{g}'_M = \mathbf{P}\mathbf{G}^{1/2}\mathbf{g}'$
$\mathbf{H}'_M = \mathbf{G}^{1/2}\mathbf{H}'\mathbf{G}^{1/2}$	${}^{IS}\mathbf{H}'_M = \mathbf{P}\mathbf{G}^{1/2}\mathbf{W}_{IS}'\mathbf{G}^{1/2}\mathbf{P} + (\mathbf{1}-\mathbf{P})\mathbf{A}(\mathbf{1}-\mathbf{P})$
$\mathbf{p}'_M = \mathbf{G}^{-1/2}\mathbf{p}'$	${}^{IS}\mathbf{p}'_M = \mathbf{P}\mathbf{G}^{-1/2}\mathbf{p}'$

[a] See eq 6. **G** is the Wilson matrix;[41] **g**, **H**, and Δ**q** indicate the gradient, the Hessian, and the displacement, respectively.

Computation of the Minimum Energy Path within the Intersection Space. We now move to discuss the second algorithm proposed in this paper. This method permits the computation of a coordinate analogous to the intrinsic reaction coordinate (IRC), confined to the intersection space (IS-IRC). Although several methods have been proposed to compute a segment of the intersection space [see for example ref 6, 20, 26, 32, and 40 and references therein], the algorithm that we have implemented is based upon the one proposed by Gonzalez et al.[31] We will briefly present the ideas behind the original IRC algorithm, and then we will describe the modifications required to compute directly the IS-IRC.

As shown in Figure 1, the original IRC algorithm[30,31] was designed such that starting from a point $\mathbf{q}_0$, a $^1/_2s$ displacement along the gradient $\mathbf{G}\mathbf{g}_0$ is taken to locate point $\mathbf{q}_0^*$, defined as the *pivot point*. From this pivot point, a constrained optimization is carried out on the surface of a hypershere of radius $^1/_2s$ and centered at $\mathbf{q}_0^*$. Thus, in Figure 1, $\mathbf{q}_0$, $\mathbf{q}'$ and $\mathbf{q}$ are three points on the hypersphere and $\mathbf{q}_0^*$ the center of it. Along the reaction path, at every $\mathbf{q}$ the residual gradient is, by construction, parallel to the $\mathbf{p}$ vector. Using this observation and the fact that the radius of the hypersphere must equal $^1/_2s$, one obtains the following set of equations

$$\Delta\mathbf{q}_M = -(\mathbf{H}_M - \sigma\mathbf{I})^{-1}(\mathbf{g}_M - \sigma\mathbf{p}_M) \tag{6a}$$

$$\Delta\mathbf{q}_M^T\Delta\mathbf{q}_M = [\mathbf{p}_M - (\mathbf{H}_M - \sigma\mathbf{I})^{-1}(\mathbf{g}_M - \sigma\mathbf{p}_M)]^T[\mathbf{p}_M - (\mathbf{H}_M - \sigma\mathbf{I})^{-1}(\mathbf{g}_M - \sigma\mathbf{p}_M)] = (1/2s)^2 \tag{6b}$$

where the scalar σ is the Lagrange multiplier, **I** is the identity matrix and the remaining quantities are defined in Table 2.

In order to compute the intersection space path, we follow the same derivation. However, all the quantities previously

introduced are now projected onto the intersection space using the **P** matrix defined in eq 2d. Thus, replacing the various terms in eq 6 (Table 2), the intersection-space displacement, $\Delta\mathbf{q}_{IS}$, can be computed. However, due to the curved nature of the intersection space (see for instance refs 1, 8, 9, 36, and 42), this displacement will in general make the two crossing surfaces split apart. To restore the degeneracy, an additional displacement within the branching space is finally added, in the spirit of the algorithm described above and in the way that has been defined in eq 4c. As we will discuss in the next section, we have imposed convergence criteria on both gradient and displacement computed. Consequently, the degeneracy condition is implicitly required from eq 4c, since a large displacement would correspond to a large energy gap.

3. Computational Details

The two algorithms described in the previous section have been implemented in a development version of the Gaussian package[28] and at the state averaged complete active space self-consistent field level of theory (SA-CASSCF). Nevertheless, they can be easily implemented at any other level of theory, provided that analytical energy gradients and the nonadiabatic interstate coupling vector are available. The overall convergence of the algorithm to optimize conical intersections has been tested on the S_0/S_1 crossing seam of benzene. The calculations have been carried out at the SA-CASSCF level of theory, with a six π electrons and six π orbitals active-space and an STO-3G basis set. An active space of (6π, 6π) and one of (4π, 4π) were instead used to investigate the S_0/S_1 crossing seams of *z*-penta-3,5-dieniminium and 1,3-butadiene, respectively. Also in these examples we have used the 2-SA-CASSCF level of theory, but with a 6-31G* basis set. All energies in the figures are reported in hartree (E_h).

In all the examples presented, the two crossing electronic states were equally weighted and the coupled perturbative MCSCF (CP−MCSCF) equations solved to evaluate the gradients (see for instance ref 43). However, tests have been also carried out using approximate gradients, i.e., without solving the CP−MCSCF equations, to guarantee the efficiency of the code implementation for molecules with either a large active space or a large number of atoms, where it may be too expensive to solve the CP−MCSCF equations. In these tests, the same structures (within 0.5 kcal mol^{-1}) were optimized with and without computing the corrections for the gradients. Nevertheless, we have noticed that away from the seam region, the two optimizations may differ significantly. This had some consequences for 1,3-butadiene, which has a complex intersection space with a large number of local minima. There the displacement computed with the approximate gradient can lead to a different stationary point if the optimization starts far away from the seam region.

In the examples considered in the next section, a conical intersection geometry is considered converged when the largest component of the intersection-space gradient, or of ${}^{IS}\mathbf{g'_M}$ (Table 2) for the second algorithm, is smaller than 4.5×10^{-4} au and with rms below 3.0×10^{-4} au. In addition to the gradient, also the maximum component of the total displacement is checked, $\Delta\mathbf{q}_0$ in eq 4c. A geometry is thus considered converged when the largest component of such a displacement is smaller than 1.8×10^{-3} au with rms 1.2×10^{-3} au.

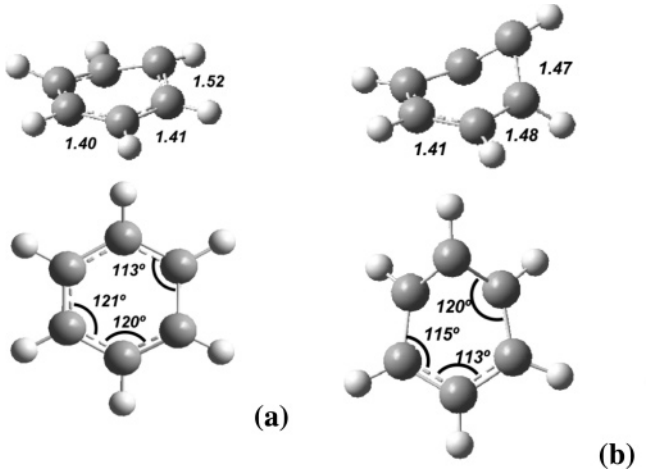

Figure 2. Starting benzene geometry **(a)** and optimized S_0/S_1 conical intersection geometry **(b)** at the SA-CASSCF(6,6)/STO-3G level. All the angles (*italic*) are reported in degrees, while C−C bonds are reported in Å.

In the last example reported below, we map out a finite portion of the S_0/S_1 1,3-butadiene crossing seam. Due to the complex morphology of the area around the conical intersection ${}^{SP}\mathbf{CI}_{66}$, in our computations the step length was reduced. This explains the number of points on the left-hand side of the profile in Figure 9a.

Finally, we should point out all the conical intersection points discussed in this work have a peaked topology,[7] but the algorithm reported has also been tested on sloped conical intersections.

4. Results and Discussions

The purpose of this section is to illustrate the potential of the two algorithms described in section 2. We begin by comparing the performance of the proposed conical intersection search algorithm using the S_0/S_1 and S_0/T_1 crossing seams of benzene. The *z*-penta-3,5-dieniminium crossing seam will be used as an example of constrained optimization. Finally, the S_0/S_1 crossing seam of butadiene is examined by optimizing a saddle point on this hyperline, then computing the associated intersection-space path.

Conical Intersection Algorithm. To evaluate the overall efficiency of the conical intersection algorithm, the S_0/S_1 conical intersection seam of benzene (see for example refs 44 and 45) has been used. We compare here the global convergence of the benzene S_0/S_1 conical intersection optimization computed by using the algorithm of Bearpark et al.,[14] the one proposed by Anglada et al.[22] and the one proposed in this paper. All the conical intersection optimizations were started from a slightly nonplanar benzene structure obtained by distorting the minimum geometry (Figure 2a) on the S_1 potential energy surface.[44]

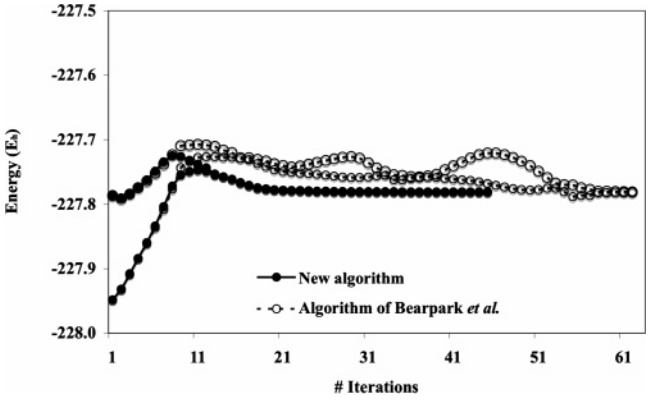

Figure 3. Global convergence of an S_0/S_1 conical intersection optimization of a benzene molecule: comparison between the energy profiles obtained by the algorithm of Bearpark et al. (open circles) and the proposed algorithm (filled circles).

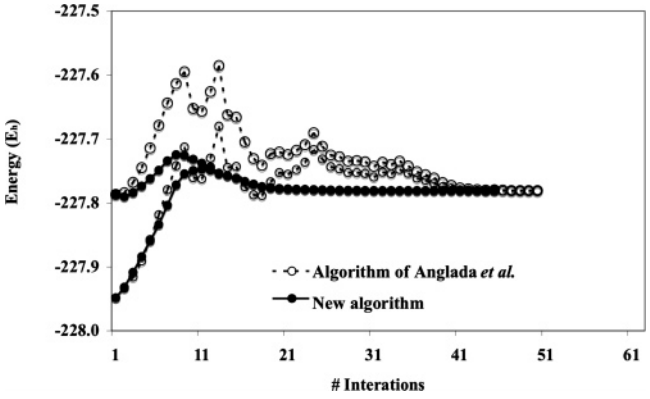

Figure 4. Global convergence of an S_0/S_1 conical intersection optimization of benzene: comparison between the method introduced by Anglada et al. (open circles) and the proposed algorithm (filled circles).

The same conical intersection geometry was optimized by the three different algorithms (Figure 2b), which is that previously reported by Bearpark et al.[14] As noted in that study, a bigger basis set would, on one hand, provide a more accurate description of the molecular geometry. On the other hand, a bigger basis would not invalidate the results obtained regarding the convergence behavior. The objective of the test presented here is to discuss the total convergence of the new algorithm, so we used a relatively small basis set to speed up the tests.

In Figures 3 and 4 we show the energy changes of the two S_0 and S_1 crossing states for benzene computed with the three algorithms during the optimization. As discussed in section 2, the algorithm of Bearpark et al. (open circles in Figure 3) promptly reaches the crossing seam. However, once in that region, a poorly conditioned Hessian slows the overall convergence. On the other hand, the algorithm proposed by Anglada et al. has a slower convergence toward the crossing seam (open circles in Figure 4) but gives a much smoother profile in the degeneracy region. In addition to the low rate of convergence to the degeneracy region, this latter algorithm tends to take steps in high-energy regions, where

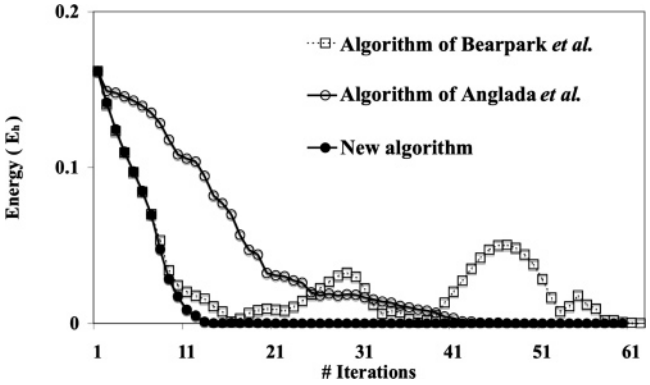

Figure 5. Energy difference between the S_0 and S_1 electronic states in benzene during the conical intersection optimization.

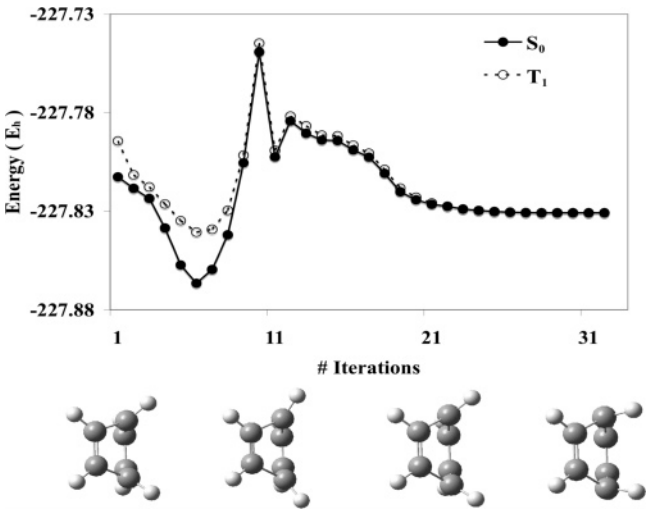

Figure 6. Global convergence of the optimization of an S_0/T_1 crossing geometry of benzene using the new algorithm presented here. Geometries for selected points (1, 11, 21, 31) along the optimization path are shown at the bottom of the figure.

Scheme 1

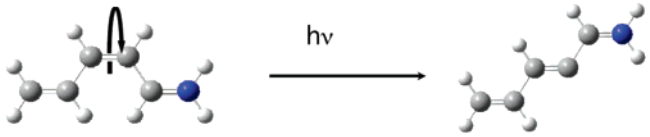

other molecules may, for example, dissociate and therefore be channeled toward high-energy portions of the intersection seam.

It is easily appreciated that the new algorithm (filled circles and solid line in both Figures 3 and 4) has a faster convergence, when compared with both the other methods. In addition, it is clear that the new algorithm combines the strengths of the two methods in different regions of the optimization: it has the fast convergence rate in the first part of the optimization, but it is also able to maintain the degeneracy between the two crossing electronic states once the crossing seam is reached.

To emphasize this last point, in Figure 5, the difference of the energies of the S_0 and S_1 states of benzene during the intersection optimization is shown. It should be noted that the starting geometry is very poor, since the initial energy

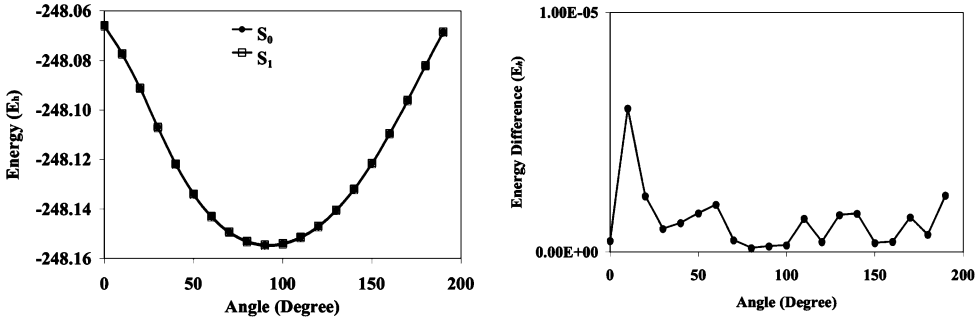

(a) (b)

Figure 7. Energy profile obtained as a function of the *z*-penta-3,5-dieniminium cation central bond rotation **(a)**. The degeneracy is reached for all the examined angles as shown in panel **(b),** where the energy difference is reported.

gap between the two states is over 100 kcal mol^{-1}. Such a difficult test demonstrates the robust global convergence of all three algorithms. The algorithm presented here shows a faster decrease of the energy gap.

Our new algorithm is also able to optimize crossing points along (*n*-1)-dimensional crossing seams. In Figure 6, we show, as an example, the energy separation and the geometrical changes during the optimization of a crossing point on the T_1/S_0 crossing seam of benzene. As initial geometry (iteration 1 in Figure 6), we have used a boat-like structure, resembling the transition state connecting benzene to Dewar benzene.[44,46] Also in this type of crossing, the algorithm presented in this paper shows a robust overall convergence and promptly approaches the crossing seam. We note that the crossing point optimized in this test differs from the geometry obtained in our previous study,[14] as a consequence of choosing a different starting geometry.

To illustrate the generality of our implementation, we now show a constrained conical intersection optimization within the S_0/S_1 intersection space of *z*-penta-3,5-dieniminium cation.[26,47] We have carried out a relaxed scan of the central dihedral angle (Scheme 1), and in Figure 7a we report the energy profile computed. As previously reported,[26,32,47,48] we have found the minimum crossing point to be in the region of 90°. However, it should be noted that the new algorithm can achieve a high level of degeneracy (see for instance refs 26 and 32) at all the optimized structures (Figure 7b).

Algorithm To Compute the Intersection-Space Minimum Energy Path. To further demonstrate the generality of the proposed conical intersection algorithm, we have optimized a saddle point along the S_0/S_1 crossing seam of 1,3-butadiene. Such a saddle point is then linked up with two structures lower in energy, along an intersection space minimum energy path computed with the second proposed algorithm.

Generally, in order to optimize a saddle point structure, one must start from a geometry that is close enough to the quadratic region of such a point. In addition, the Hessian at this initial structure must show a negative eigenvalue, and the corresponding eigenvector must be a suitable approximation for the direction connecting the two valleys. When one tries to optimize a saddle point within the

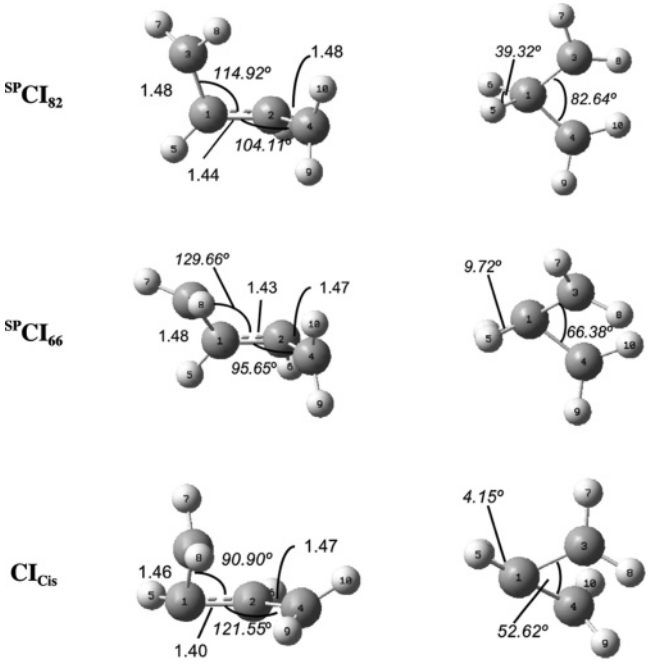

Figure 8. Important geometric parameters for the optimized butadiene CI geometries found along the S_0/S_1 1,3-butadiene crossing seam. The bond lengths are expressed in Å, while the angles (in *italic*) are presented in degrees.

intersection space, the initial geometry should also be a point of degeneracy, since the intersection-space Hessian must be computed.

In our first studies[13,49] on 1,3-butadiene, we optimized three stationary points along the S_0/S_1 crossing seam: the *cisoidal*, the *transoidal*, and the *central* structure. In the present study, starting from the *central* geometry we first re-optimized the energy gap between the two states along the gradient difference vector. At this point on the conical intersection seam, the intersection-space Hessian was computed and an imaginary frequency (with corresponding eigenvector) obtained. Finally, using the new algorithm presented in this paper, we were able to optimize a new saddle point not reported previously (^{SP}**CI**$_{82}$ in Figure 8). This structure shows an imaginary frequency of 639 *i* cm^{-1} corresponding to a combination of a -CH_2 twisting mode and a symmetric rocking mode localized on H_5 and H_6. It closely resembles the ^{SP}**CI**$_{cis/cis}$ structure previously reported

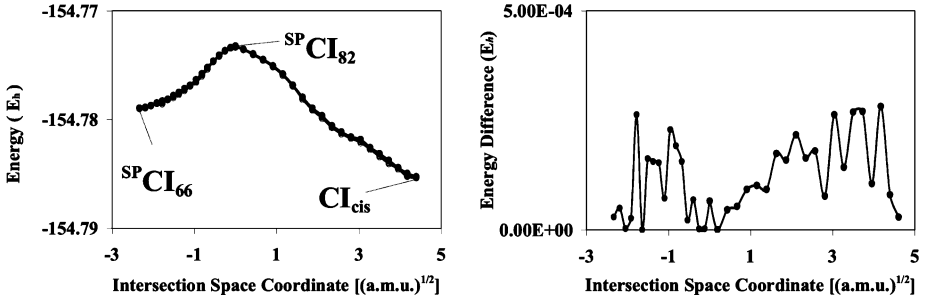

Figure 9. Minimum energy path connecting ^{SP}**CI$_{66}$** (negative part of the intersection space coordinate in panel **a**) to the **CI$_{CIS}$** (positive intersection coordinate in panel **a**) through ^{SP}**CI$_{82}$**. In panel (**b**), the energy difference computed at each point along the intersection space minimum energy coordinate is reported.

elsewhere,[9] but where the C_2 symmetry has been broken and consequently a slightly lower (<1 kcal mol^{-1}) energy is obtained.

In Figure 9, we report the results obtained with the algorithm designed to compute the minimum energy path within the intersection space, discussed in section 2.

We started our intersection-space minimum energy path computation from the structure ^{SP}**CI$_{82}$** (Figure 8), and we have used as initial relaxation direction (see for instance refs 10, 30, 31, and 50) the eigenvector corresponding to the imaginary frequency. The accuracy of the algorithm proposed in this paper can be appreciated from Figure 9b, which shows that the energy difference at each optimized structure along the path is well below 1 kcal mol^{-1}.

Our results show that ^{SP}**CI$_{82}$** connects one of the *s-cisoidal* conical intersection isomers (**CI$_{Cis}$** in Figure 8) with a new conical intersection saddle point (^{SP}**CI$_{66}$** in Figure 8). The absence of discontinuity in this profile (Figure 9a) is evidence of a single crossing seam. The calculated coordinate is somewhat unconventional as it ends at a saddle point, ^{SP}**CI$_{66}$**, but the imaginary frequency at ^{SP}**CI$_{66}$** is perpendicular to the intersection space coordinate that connects ^{SP}**CI$_{82}$** to ^{SP}**CI$_{66}$**. A similar case was described in our previous butadiene study,[9] which is an indication of the complexity of the intersection space, even for an apparently simple example such as butadiene.

4. Conclusions

In this paper we presented two new algorithms to study the extended nature of the crossing seam between two electronic potential energy surfaces. The first algorithm represents an improvement over the algorithms already available. It combines fast convergence in reaching the seam region with flexibility in the degeneracy region itself. To demonstrate the potential of this algorithm, we have optimized both minima and saddle points on crossing seams as well as carried out conical intersection optimization with a frozen internal coordinate. In all cases, the results obtained show a fast and smooth convergence to an optimized conical intersection point.

The second algorithm has instead been designed to compute the intersection-space minimum energy path. Adapting one of the available algorithms[31] to compute the reaction path on a single potential energy surface, we have implemented an analogous method limited exclusively to the intersection space. We have shown its potential by explicitly mapping out a finite region of the S_0/S_1 1,3-butadiene crossing seam.

Acknowledgment. L.B. is financed by the Spanish/ Ministerio de Educación y Ciencia/ for Project No. CTQ2005-04563 and the Ramón y Cajal program. F.S. is pleased to acknowledge the support of Gaussian, Inc. and the grant given by ESF-COST P9, Radiation Damage in Biological Systems, for sponsoring his visit to the University of Girona.

Appendix

In this Appendix, we will show the equivalence between the gradient of one of the two crossing states energy and the average gradients, once they are both projected onto the first-order intersection space. Using the definition of projection matrix given in eq 2c, the projected gradient, for instance, of the state 2 can be written as

$$\mathbf{P}\frac{\partial E_2}{\partial \mathbf{q}} \tag{A.1}$$

On the other hand, the projected average gradient is defined as

$$\frac{1}{2}\mathbf{P}\frac{\partial (E_2 + E_1)}{\partial \mathbf{q}} \tag{A.2}$$

Proving their difference zero is equivalent to show that they are the same vector. Thus

$$\frac{1}{2}\mathbf{P}\frac{\partial (E_2 + E_1)}{\partial \mathbf{q}} - \mathbf{P}\frac{\partial E_2}{\partial \mathbf{q}} = \frac{1}{2}\mathbf{P}\frac{\partial (E_1 - E_2)}{\partial \mathbf{q}} = \frac{1}{2}\mathbf{P}\mathbf{x}_1 = \frac{1}{2}(\mathbf{x}_1 - \mathbf{x}_1) = \mathbf{0} \tag{A.3}$$

In eq A.3, we have used the definition of the projection matrix **P** [eq 2] and exploited the fact that the gradient difference vector and the nonadiabatic interstate coupling vectors are chosen to be orthonormal to each other.

References

(1) Domcke, W.; Yarkony, D. R.; Koppel, H. *Conical Intersections: Electronic Structure, Dynamics & Spectroscopy*; World Scientific Publishing Co.: Singapore, 2004.

(2) Bernardi, F.; Olivucci, M.; Robb, M. A. *Chem. Soc. Rev.* **1996**, *25*, 321; Klessinger, M.; Michl, J. *Excited States and Photochemistry of Organic Molecules*; Wiley-VCH: New York, 1995.

(3) Yarkony, D. R. *Rev. Mod. Phys.* **1996**, *68*, 985.

(4) Toniolo, A.; Levine, B.; Thompson, A.; Quenneville, J.; Ben-Nun, M.; Owens, J.; Olsen, S.; Manohar, L.; Martinez, T. J. Photochemistry from First Principles and Direct Dynamics in Computational Methods. In *Computational Methods in Photochemistry*; Kutateladze, A., Ed.; CRC Press: Boca Raton, 2005; pp 166−234.

(5) Ben-Nun, M.; Martinez, T. J. *Chem. Phys. Lett.* **1998**, *298*, 57. Boggio-Pasqua, M.; Bearpark, M. J.; Hunt, P. A.; Robb, M. A. *J. Am. Chem. Soc.* **2002**, *124*, 1456. Boggio-Pasqua, M.; Bearpark, M. J.; Ogliaro, F.; Robb, M. A. *J. Am. Chem. Soc.* **2006**, *128*, 10533. Boggio-Pasqua, M.; Ravaglia, M.; Bearpark, M. J.; Garavelli, M.; Robb, M. A. *J. Phys. Chem. A* **2003**, *107*, 11139.

(6) Laino, T.; Passerone, D. *Chem. Phys. Lett.* **2004**, *389*, 1.

(7) Atchity, G. J.; Xantheas, S. S.; Ruedenberg, K. *J. Chem. Phys.* **1991**, *95*, 1862.

(8) Paterson, M. J.; Bearpark, M. J.; Robb, M. A.; Blancafort, L. *J. Chem. Phys.* **2004**, *121*, 11562; Sicilia, F.; Blancafort, L.; Bearpark, M. J.; Robb, M. A. *Theor. Chem. Acc.* **2007**, *118*, 241.

(9) Sicilia, F.; Blancafort, L.; Bearpark, M. J.; Robb, M. A. *J. Phys. Chem. A* **2007**, *111*, 2182.

(10) Schlegel, H. B. *J. Comput. Chem.* **2002**, *24*, 1514.

(11) Yarkony, D. R. *J. Chem. Phys.* **1990**, *92*, 2457.

(12) Dallos, M.; Lischka, H.; Shepard, R.; Yarkony, D. R.; Szalay, P. G. *J. Chem. Phys.* **2004**, *120*, 7330.

(13) Ragazos, I. N.; Robb, M. A.; Bernardi, F.; Olivucci, M. *Chem. Phys. Lett.* **1992**, *197*, 217.

(14) Bearpark, M. J.; Robb, M. A.; Schlegel, H. B. *Chem. Phys. Lett.* **1994**, *223*, 269.

(15) Chachiyo, T.; Rodriguez, J. H., *J. Chem. Phys.* **2005**, *123*, 094711; Yamazaki, S.; Kato, S. *J. Chem. Phys.* **2005**, *123*, 114510. Izzo, R.; Klessinger, M. *J. Comput. Chem.* **2000**, *21*, 52. Page, C. S.; Olivucci, M. *J. Comput. Chem.* **2003**, *24*, 298.

(16) Fletcher, R. *Practical Methods of Optimization*; Wiley & Sons: New York, 1981; Vol. 2.

(17) Gill, P. E.; Murray, W. *Numerical Methods for Constrained Optimization*; Academic Press: London, 1974.

(18) Manaa, M. R.; Yarkony, D. R. *J. Chem. Phys.* **1993**, *99*, 5251.

(19) Keal, T. W.; Koslowski, A.; Thiel, W. *Theo. Chem. Acc.* **2007**, *118*, 837−844.

(20) De Vico, L.; Olivucci, M.; Lindh, R. *J. Chem. Theory Comput.* **2005**, *1*, 1029.

(21) Yarkony, D. R. *J. Phys. Chem.* **2004**, *108*, 3200.

(22) Anglada, J. M.; Bofill, J. M. *J. Comput. Chem.* **1996**, *18*, 992.

(23) Nocedal, J.; Overton, M. L. *SIAM J. Num. Anal.* **1985**, *22*, 821.

(24) Toniolo, A.; Ben-Nun, M.; Martinez, T. J. *J. Phys. Chem. A* **2002**, *106*, 4679.

(25) Bearpark, M. J.; Blancafort, L.; Paterson, M. J. *Mol. Phys.* **2006**, *104*, 1033.

(26) Migani, A.; Robb, M. A.; Olivucci, M. *J. Am. Chem. Soc.* **2003**, *125*, 2804.

(27) Takahashi, O.; Sumita, M., *J. Chem. Phys.* **2004**, *121*, 7030.

(28) Frisch, M. J.; Trucks, G. W.; Schlegel, H. B.; Scuseria, G. E.; Robb, M. A.; Cheeseman, J. R.; Montgomery, J. A., Jr.; Vreven, T.; Scalmani, G.; Kudin, K. N.; Iyengar, S. S.; Tomasi, J.; Barone, V.; Mennucci, B.; Cossi, M.; Rega, N.; Petersson, G. A.; Nakatsuji, H.; Hada, M.; Ehara, M.; Toyota, K.; Fukuda, R.; Hasegawa, J.; Ishida, M.; Nakajima, T.; Honda, Y.; Kitao, O.; Nakai, H.; Li, X.; Hratchian, H. P.; Peralta, J. E.; Izmaylov, A. F.; Heyd, J. J.; Brothers, E.; Staroverov, V.; Zheng, G.; Kobayashi, R.; Normand, J.; Burant, J. C.; Millam, J. M.; Klene, M.; Knox, J. E.; Cross, J. B.; Bakken, V.; Adamo, C.; Jaramillo, J.; Gomperts, R.; Stratmann, R. E.; Yazyev, O.; Austin, A. J.; Cammi, R.; Pomelli, C.; Ochterski, J. W.; Ayala, P. Y.; Morokuma, K.; Voth, G. A.; Salvador, P.; Dannenberg, J. J.; Zakrzewski, V. G.; Dapprich, S.; Daniels, A. D.; Strain, M. C.; Farkas, O.; Malick, D. K.; Rabuck, A. D.; Raghavachari, K.; Foresman, J. B.; Ortiz, J. V.; Cui, Q.; Baboul, A. G.; Clifford, S.; Cioslowski, J.; Stefanov, B. B.; Liu, G.; Liashenko, A.; Piskorz, P.; Komaromi, I.; Martin, R. L.; Fox, D. J.; Keith, T.; Al-Laham, M. A.; Peng, C. Y.; Nanayakkara, A.; Challacombe, M.; Chen, W.; Wong, M. W.; Pople, J. A. *Gaussian Development Version, Revision F.01*; Gaussian, Inc.: Wallingford, CT, 2006.

(29) Fukui, K. *Acc. Chem. Res.* **1981**, *14*, 363.

(30) Gonzalez, C.; Schlegel, H. B. *J. Chem. Phys.* **1989**, *90*, 2154.

(31) Gonzalez, C.; Schlegel, H. B. *J. Chem. Phys.* **1990**, *94*, 5523.

(32) Migani, A.; Sinicropi, A.; Ferre, N.; Cembran, A.; Garavelli, M.; Olivucci, M. *Faraday Discuss.* **2004**, *127*, 179.

(33) Yarkony, D. R. *J. Chem. Phys.* **2005**, *123*, 204101.

(34) Redmon, L. T. *Phys. Rev. A* **1982**, *25*, 2453.

(35) Mead, C. A. *J. Chem. Phys.* **1983**, *78*, 807. Young, R. A.; Yarkony, D. R. *J. Chem. Phys.* **2006**, *125*, 234301.

(36) Yarkony, D. R. *J. Chem. Phys.* **2005**, *123*, 134106.

(37) Peng, C.; Ayala, P. Y.; Schlegel, H. B.; Frisch, M. J. *J. Comput. Chem.* **1996**, *17*, 49.

(38) Wright, S. J. Algorithms and Software for Linear and Nonlinear Programming. In *Foundations of Computer-Aided Process Design*; CACHE Publications: 1999.

(39) Bofill, J. M. *J. Comput. Chem.* **1994**, *15*, 1.

(40) Passerone, D.; Laino, T. *Comput. Phys. Commun.* **2005**, *169*, 305.

(41) Wilson, E. B.; Decius, G. C.; Cross, P. C. *Molecular Vibrations*; McGraw-Hill: London, 1955.

(42) Yarkony, D. R. *J. Chem. Phys.* **2005**, *123*, 1234106.

(43) Almlöf, J.; Taylor, P. *Int. J. Quantum Chem.* **1985**, *27*, 743.

(44) Palmer, I. J.; Ragazos, I. N.; Bernardi, F.; Olivucci, M.; Robb, M. A. *J. Am. Chem. Soc.* **1993**, *115*, 673.

(45) Domcke, W.; Sobolewski, A. L.; Woywod, C. *Chem. Phys. Lett.* **1993**, *203*, 220; Sobolewski, A. L.; Woywod, C.; Domcke, W. *J. Chem. Phys.* **1993**, *98*, 5627.

(46) Turro, N. J. *Modern Molecular Photochemistry*; Benjamin Cummings: Menlo Park, CA, 1978.

(47) Garavelli, M.; Celani, P.; Bernardi, F.; Robb, M. A.; Olivucci, M. *J. Am. Chem. Soc.* **1997**, *119*, 6891. Weingart, O.; Migani, A.; Olivucci, M.; Robb, M. A.; Buss, V.; Hunt, P. *J. Phys. Chem. A* **2004**, *108*, 4685. Vreven, T.; Bernardi, F.; Garavelli, M.; Olivucci, M.; Robb, M. A.; Schlegel, H. B. *J. Am. Chem. Soc.* **1997**, *119*, 12687.

(48) Garavelli, M.; Bernardi, F.; Olivucci, M.; Vreven, T.; Klein, S.; Celani, P.; Robb, M. A. *Faraday Discuss.* **1998**, *110*, 51.

(49) Olivucci, M.; Ragazos, I. N.; Bernardi, F.; Robb, M. A. *J. Am. Chem. Soc.* **1993**, *115*, 3710.

(50) Celani, P.; Robb, M. A.; Garavelli, M.; Bernardi, F.; Olivucci, M. *Chem. Phys. Lett.* **1995**, *243*, 1.

CT7002435